Journal of Molecular Graphics and Modelling 27 (2008) 66–81

Contents lists available at ScienceDirect

Journal of Molecular Graphics and Modelling

journal homepage: www.elsevier.com/locate/JMGM

The structure of human serotonin 2c G-protein-coupled receptor bound to agonists and antagonists

Jenelle K. Bray, William A. Goddard III*

Materials and Process Simulation Center, California Institute of Technology, MC 139-74, Pasadena, CA 91125, United States

ARTICLE INFO

Article history:
Received 25 October 2007
Received in revised form 25 January 2008
Accepted 23 February 2008
Available online 27 March 2008

Keywords:
Protein structure prediction
Binding site prediction
Membrane proteins
G-protein-coupled receptors
Serotonin receptors

ABSTRACT

We used the MembStruk computational procedure to predict the three-dimensional (3D) structure for the serotonin 5-HT_{2C} G-protein-coupled receptor (GPCR). Using this structure, we used the MSCDock computational procedure to predict the 3D structures for bound ligand–protein complexes for agonists such as serotonin and antagonists such as ritanserin, metergoline, and methiothepin. In addition, we predicted the SAR data for a series of psilocybin analogs, both agonists and antagonists. We performed molecular dynamics (MD) on serotonin bound to 5-HT_{2C} and we find the protein and binding site to be stable after 5 ns. We find good agreement with the currently known experimental data and we predict a number of new mutations which could be used to validate further our predicted structures. This agreement between theory and experiment suggests that our 3D structure is sufficiently accurate for use in drug design. We also compare a preliminary prediction for 5-HT_{2B} with our prediction for 5-HT_{2C} and find a difference in TM5 that contributes to different serotonin binding modes in 5-HT_{2B} and 5-HT_{2C}.

1. Introduction

The serotonin (5-hydroxytryptamine, or 5-HT) class of G-protein-coupled receptors (GPCR) serve as neurotransmitters involved in many processes in the central nervous system, including the regulation of feeding, aggression, mood, perception, pain and anxiety [1]. Additionally, 5-HT regulates vascular and nonvascular smooth muscle growth, uterine smooth muscle growth, and gastrointestinal functioning [1]. Consequently, these receptors are targets for a variety of drug therapies. This family of receptors that consists of at least 15 receptors partitioned into seven main types, helps to mediate these physiological functions. This creates a problem for drug design since all 15 likely have similar binding sites, making it difficult to attain selectivity of a drug to just one receptor. This problem is made worse because there are no 3D X-ray structures for any of these receptors. To help fill this gap we have been developing methods (MembStruk) for predicting the 3D structures.

We consider here the 5-HT_2 family, which consists of three structurally related receptors: 5-HT_{2A}, 5-HT_{2B} and 5-HT_{2C}. Drugs that target 5-HT_2 receptors are used to treat such disorders as schizophrenia, depression and glaucoma. The three 5-HT_2 receptors have high sequence identity within the transmembrane domains, and they play a variety of physiological roles. The majority of current drugs with affinity for 5-HT_2 receptors are not subtype specific [2], so it is often unclear which receptor is responsible for the particular physiological effect and which receptor is responsible for unwanted side effects. We expect that detailed knowledge of the ligand-binding environment of the 5-HT_2 receptors would facilitate the creation of more subtype specific drugs that in turn would lead to a better understanding of the specific physiological role of each receptor.

Since no direct studies have determined how ligands bind to 5-HT_2 receptors [1], we will use computational methods to predict the 3D structure of the receptors and of the ligand–receptor complexes. Since there are no experimental structures for comparison, we validate our predicted structures indirectly by comparison with available mutagenesis and ligand-binding experiments. Then we predict the results for new mutation and binding studies that could be carried out experimentally. We report here the results for 5-HT_{2C}, and preliminary results for 5-HT_{2B}. These studies should provide the data needed to design subtype-specific drugs and to determine the origin of physiological responses to different agonists and antagonists.

The 5-HT_{2C} receptors are found in many regions of the brain. Some evidence suggests that 5-HT_{2C} may play a role in the mediation of the sleep–wake cycle [2]. The activation of 5-HT_{2C} appears also to be correlated with penile erections [2]. Several studies have suggested a prominent role for 5-HT_{2C} receptors in the regulation of food intake and energy balance, and that 5-HT_{2C} agonists act as appetite suppressants [3]. Additionally, 5-HT_{2C} is believed to be involved in anxiety, feeding behaviors, and anxiety-related

* Corresponding author. Tel.: +1 626 395 3093; fax: +1 626 585 0918.
E-mail address: wag@wag.caltech.edu (W.A. Goddard III).

1093-3263/$ – see front matter © 2008 Elsevier Inc. All rights reserved.
doi:10.1016/j.jmgm.2008.02.006

disorders like obsessive–compulsive disorder (OCD) [3]. In fact, 5-HT_{2C} agonists can intensify the symptoms of schizophrenia and OCD. However, it is difficult to determine whether these symptoms are caused solely by 5-HT_{2C} activation because the activation of other 5-HT receptors, most notably 5-HT_{2A}, is implicated in similar physiological effects [3].

In order to provide the basis for designing subtype-specific agonists and antagonists for the 5-HT_{2C} receptor, we set out to obtain the 3D structure of this receptor and for ligands binding to it. We did not use homology modeling because of the two experimentally known 3D structure for GPCRs, 5-HT_{2C} is only 19% homologous to bovine rhodopsin [4] and 31% homologous to the beta(2)-adrenergic receptor, whose structure has been recently solved [5]. Additionally, we have found in studies of other GPCRs that systems with even 80% sequence identity can have different binding sites. Instead, we used the MembStruk GPCR structure prediction procedure to predict the 3D structure. MembStruk has been used successfully to predict the structures for CCR1 chemokine receptor, MrgC11 tetrapeptide receptor and DP prostanoid receptor, in each case for which experimental validation was done after the predictions. In addition, predictions of the structures for D2 dopamine receptor, β2 adrenergic receptor and M1 muscarinic acetylcholine receptor are in good agreement with numerous mutation and ligand-binding experiments. Furthermore, predictions of olfactory receptors, the PTC bitter-taste receptor, and rhodopsin agree with somewhat more limited ligand-binding experiments [6–14].

Here we report the structure prediction for the 5-HT_{2C} receptor, and then we use the MSCDock procedure [15] to predict the binding sites of serotonin and three strongly binding antagonists. In addition, we predict the binding of 10 psilocybin analogs to compare with experimental SAR data. We also compare the predicted structure for 5-HT_{2C} with a preliminary prediction of 5-HT_{2B}. In all cases, we obtain excellent agreement with currently available data and we predict new experiments to validate further the predicted structures.

2. Methodology

We used the MembStruk procedure (Version 4.30) [11,14] to predict the structure of the 5-HT_{2C} receptor. This procedure consists of five main steps:

(1) Prediction of the transmembrane (TM) helices from hydrophobic analyses of the amino acid sequence.
(2) Assembly of the seven helix TM bundle and coarse grain optimization of the bundle.
(3) Rigid body dynamics of the bundle in an explicit lipid bilayer.
(4) Optimization of individual helices.
(5) Optimization of the entire protein.

Throughout these steps, MPSim [16] was used with the Dreiding forcefield [17] for the molecular mechanics and molecular dynamics steps unless otherwise specified, with a dielectric constant of 2.5, and a 6–12 Lennard–Jones potential for the van der Waals interactions.

2.1. TM predictions

The prediction of the TM helical regions is based on the assumption that the outward facing sections of the TM helices must be hydrophobic because they are in contact with the hydrocarbon tails of the lipid bilayer, and that the hydrophobic center of each helix should be at the center of the membrane [18]. These ideas are used in the TM2ndS program to determine the TM helical regions with a hydrophobic profile and helical capping rules. To determine the hydrophobic profile, sequences related to 5-HT_{2C} were found with NCBI BLAST [19]. Of the ~200 sequences, we selected an ensemble of ~100 sequences having a uniform distribution of sequence identities from 20 to <100%. These sequences (including the target) were aligned with ClustalW to generate pairwise multiple sequence alignments [20]. From the multiple sequence alignments, we kept only the ~40 for mouse, rat and human receptors.

We used the Eisenberg hydrophobicity scale [21] (which assigns each amino acid a hydrophobicity value ranging from −1.76 to 0.73) to estimate the hydrophobicity for each residue position in the alignment and we averaged this over all of the sequences in the multiple sequence alignment. The Eisenberg scale was used because we validated our TM predictions on bovine rhodopsin using this hydrophobicity scale [11]. Then, we calculated the hydrophobic profile by averaging the hydrophobicity over a range of window sizes ranging from 12 to 20, and selected the lowest window size that gives seven peaks with lengths greater than 20 residues. The baseline value is the average hydrophobicity over all of the amino acids in the protein, which for 5-HT_{2C} is 0.007. Because the TM helices can extend past the membrane surface, we use capping rules to refine the helix predictions. Known helix breakers are proline, glycine, arginine, histidine, lysine, aspartic acid and glutamic acid. If any such helix breakers are found within four residues toward the membrane, we keep the initial TM helix predictions. If no helix breaker is found, the helix is extended until a breaker is found, but only up to six residues. Additionally, the capping rules include the requirement that the intracellular and extracellular loops consist of at least six residues. Then we define the hydrophobic center of each TM helix as the point of maximum hydrophobicity averaged over the range of window sizes. The hydrophobic profiles and TM helix predictions, before and after capping, for 5-HT_{2C} are shown in Supplementary material.

The edges of some of the TM helices were not well defined, without any residues left to form a loop between TM2 and TM3. Thus, to further refine the predictions, each individual TM helix was BLAST searched separately. For each helix, we consider the ten residues on either side of the hydrophobic center and make a new BLAST search over the GPCR database to obtain a new set of sequences (>20% identity) and then we did a new alignment with these sequences as input to the TM2ndS program. Next, the peak for the specific helix was examined, along with capping rules, to determine the edges of the helix. The hydrophobic centers calculated with the entire protein sequence in the previous step were retained. The predictions, before and after individual helical refinement and helical capping, are given in Table 1.

Table 1 shows that the final TM predictions were taken to be the capped individual helix predictions, except for the case of TM5. Here, the capping procedure added six residues to TM5, which we considered to make the helix too long, especially in comparison to helix 5 of 5-HT_{2B}. Thus, we adjusted the prediction for helix 5 to end at a tyrosine.

2.2. Packing of the TM helices into a seven-helix bundle

The seven TM helices predicted by TM2ndS were next built into a TM bundle. First, we built each TM helix into a canonical right-handed alpha helix with extended side-chain conformations. Then we placed each so that all seven have their calculated hydrophobic centers in an imaginary plane running through the center of the lipid bilayer.

We orient the most hydrophobic face of each helix to point away from the center of the bundle (based on equal weight for each center) because we expect that it will be energetically favorable for

Table 1
TM helix predictions for 5-HT_{2C}

TM	Predicted TM Region	Prediction Method
1	GVQNWPALSIVIIIIMTIGGNILVIMA	Full protein, uncapped
	GVQNWPALSIVIIIIMTIGGNILVIMAVSME	Full protein, capped
	GVQNWPALSIVIIIIMTIGGNILVIMA	Indiv. helix, uncapped
	GVQNWPALSIVIIIIMTIGGNILVIMAVSME	Indiv. helix, capped
	GVQNWPALSIVIIIIM[T]IGGNILVIMAVSME	Final Prediction
2	YFLMSLAIADMLVGLLVMPLSLLAILYD--Y	Full protein, uncapped
	ATNYFLMSLAIADMLVGLLVMPLSLLAILYD--	Full protein, capped
	NYFLMSLAIADMLVGLLVMPLSLLAILYDY	Indiv. helix, uncapped
	TNYFLMSLAIADMLVGLLVMPLSLLAILYD	Indiv. helix, capped
	TNYFLMSLAIADM[L]VGLLVMPLSLLAILYD	Final Prediction
3	PRYLCPVWISLDVLFSTASIMHLCAISLDR	Full protein, uncapped
	RYLCPVWISLDVLFSTASIMHLCAISLDR	Full protein, capped
	PRYLCPVWISLDVLFSTASIMHLCAISLDR	Indiv. helix, uncapped
	RYLCPVWISLDVLFSTASIMHLCAISLDR	Indiv. helix, capped
	RYLCPVWISLDVLFS[T]ASIMHLCAISLDR	Final Prediction
4	MKIAIVWAISIGVSVPIPVIG	Full protein, uncapped
	IMKIAIVWAISIGVSVPIPVIGL	Full protein, capped
	IMKIAIVWAISIGVSVPIPVIG	Indiv. helix, uncapped
	AIMKIAIVWAISIGVSVPIPVIGL	Indiv. helix, capped
	AIMKIAIVWAI[S]IGVSVPIPVIGL	Final Prediction
5	FVLIGSFVAFFIPLTIMVITYCL	Full protein, uncapped
	FVLIGSFVAFFIPLTIMVITYCLTIYVLR	Full protein, capped
	FVLIGSFVAFFIPLTIMVITYCL	Indiv. helix, uncapped
	FVLIGSFVAFFIPLTIMVITYCLTIYVLR	Indiv. helix, capped
	FVLIGSFVAFF[I]PLTIMVITYCLTIY	Final Prediction
6	LGIVFFVFLIMWCPFFITNILSVLC	Full protein, uncapped
	LGIVFFVFLIMWCPFFITNILSVLCE	Full protein, capped
	LGIVFFVFLIMWCPFFITNILSV	Indiv. helix, uncapped
	LGIVFFVFLIMWCPFFITNILSVLCE	Indiv. helix, capped
	LGIVFFVFLI[M]WCPFFITNILSVLCE	Final Prediction
7	EKLLNVFVWIGYVCSGINPLVYT	Full protein, uncapped
	EKLLNVFVWIGYVCSGINPLVYT	Full protein, capped
	EKLLNVFVWIGYVCSGINPLVYT	Indiv. helix, uncapped
	EKLLNVFVWIGYVCSGINPLVYT	Indiv. helix, capped
	EKLLNVFVWIGYV[C]SGINPLVYT	Final Prediction

The predictions are given for both the initial predictions based on the full protein sequence and for the subsequent prediction in which each TM region was searched and aligned individually. In each case, the predictions are based on hydrophobicity and supplemented with predictions based on capping rules. A gap (–) in a sequence is caused by the multiple sequence alignment. In the final predictions, the calculated hydrophobic center for each helix is indicated by a boxed residue.

the most hydrophobic part of each helix to be facing outwards towards the hydrophobic lipid bilayer. This is achieved by calculating the hydrophobic moment of each helix, considering the 15 residues on either side of the hydrophobic center, but including just the face of the helix (considering 180° of the projection on a plane perpendicular to the helical axis). The hydrophobic moment is pointed outward from the center of mass of the protein.

The calculation of the center fixes the z coordinate for each helix, while the rotational orientation determines the χ angle. There remain four other parameters to uniquely position each helix: the x and y position in the plane through the center of the lipid, the tilt θ of the helix from the z axis perpendicular to the plane, and the azimuthal angle φ for the tilting plane. These four parameters we take from the 7.5 Å electron density map of frog rhodopsin [22]. This electron density map gives the relative orientations of the helical axes, but no information about translation or rotation of the helices. The original MembStruk was developed using frog rhodopsin because there was no bovine rhodpsin X-ray available at that time. We found that frog rhodopsin worked well and saw no need to change. Only the overall xy position and tilt (θ, φ) is used from the template. No detailed atom information is used. Thus we use only undifferentiated electron density information from experiment. We can take these parameters from any crystal structure or from the structure of a predicted GPCR structure after explicit lipid bilayer dynamics.

The six parameters x, y, z, θ, φ, and χ for each helix uniquely determine how to pack the seven helices into the bundle. Next, we

need to determine the structure within each helix. First, we used SCRWL [23] to place each side-chain appropriate for the seven-helix bundle. Then, we inserted counterions to offset the charged residues not in salt bridges.

2.3. Rigid body dynamics of the bundle in an explicit lipid bilayer

In order to allow the helices to deviate from ideal alpha helix structure, as is experimentally observed in transmembrane helices, we carried out torsional molecular dynamics (NEIMO MD) [24] for each individual helix at 300 K for 500 ps. The helices with prolines form bends due to the disruption of the alpha helix hydrogen bonding network. The lowest energy structure from the last 250 ps was chosen and minimized (using conjugate gradients). Then, all seven minimized helices were bundled together again by CRMS matching the structures back on to the original positions. The side-chains were then reassigned using SCRWL, and the entire bundle was minimized. Finally, the helices were again optimized rotationally and translationally as described in the previous step.

2.4. Optimization of individual helices within the bundle

Although the hydrophobic nature of the hydrocarbon tails in the membrane are important in determining the rotational orientation of the helices, interhelical hydrogen bonds and salt bridges also help stabilize the structure. Residues conserved across all biogenic amine receptors are expected to be involved in these hydrogen bonding interactions, playing a role in stabilization, binding, and/or activation. Accordingly, it is likely that they will be facing in towards the bundle in order to interact with the ligand or other helices. Moreover, TM helix 3 is near the center of the helical bundle, and hence it is less affected by the membrane environment than the other helices. Consequently, orientation by hydrophobic moment is less appropriate for helix 3. Thus, we carried out subsequent optimization of the rotational orientation of the helices by using energy minimization techniques.

Starting with the phobic face orientation, we use energy minimization to optimize the rotation of each helix. Here, each helix is rotated and optimized through a range of angles. For each angle, the helices are rotated in the order 3, 2, 1, 7, 6, 5, and 4, starting with the inner helix 3 for which the phobic face orientation is least likely to be optimum (because it interacts least with the hydrophobic membrane). The procedure is as follows: The first helix is rotated 5° and -5°, and for these angles, the side-chain positions of all seven helices are reassigned using SCRWL and the energy of the active helix is minimized (conjugate gradients) in the field of all of the other helices (whose atoms are kept fixed). The lowest energy conformation for the helix at 0°, 5° or -5° is chosen, and the helix fixed at this angle. Then, in succession, each of the other six helices is put through the same $\pm5^\circ$ rotation procedure with the other helices fixed. After all seven helices have been rotated $\pm5^\circ$ and fixed in their lowest energy conformation, the same procedure is repeated for increments of $\pm10^\circ$. This process is repeated with 5° increments up to $\pm25^\circ$. Then the process is continued with the angles decreased by 5° increments back down to $\pm5^\circ$, where at each level all helices are allowed to adjust to the environment of the other helices. The net rotations accomplished by this process for helices 1 through 7 are

$0^\circ, 5^\circ, -10^\circ, 5^\circ, 55^\circ, 0^\circ,$ and 10°.

After selecting this lowest energy rotation, the entire helical bundle is energy minimized.

The helical bundle attained by energy-based rotation in the previous step is next immersed in a lipid bilayer made up of 52 explicit DLPC molecules in two layers around the bundle. The protein is first energy minimized in this bundle, then we carry out 50 ps of rigid body dynamics at 300 K are (using MPSim) [16]. In this calculation, the helices and lipid bilayer molecules are treated as rigid bodies. This dynamics step helps to optimize the vertical helical translations and rotations in explicit lipid and to optimize the positions of the lipid molecules with respect to the helical bundle. After this simulation, we used SCRWL to replace the side-chains, now using the lipid molecules as a bump test.

Next, we again considered helical rotations, but this time each helix was rotated a full 360°, in increments of 5°, with the other six helices fixed during the entire range of rotations. For each angle, we used SCRWL to reassign side-chains, and then energy minimized all atoms of the seven helices and the explicit lipid bilayer.

For each rotated angle of a helix, the energy of the helix interacting with the six other helices is tabulated, along with the number of interhelical hydrogen bonds and the hydrophobic penalty. The hydrophobic penalty is calculated in order to ensure that it is not favorable for polar and charged residues to point into the lipid bilayer. With the lipids ignored, we consider that any residue with more than 60% of its surface area accessible to a solvent probe of radius 2.0 Å is pointing outwards toward the lipid bilayer. Then the percentage of solvent accessible surface for each residue pointing outwards within seven amino acids of the hydrophobic center is multiplied by the hydrophobicity value of the amino acid. The hydrophobicity scale used is the average of the augmented Wimley White scale [25] and the White interface scale [26]. We use this hydrophobicity scale for the hydrophobic penalty instead of the Eisenberg scale used to determine the TM regions because it is thermodynamically based, and we are performing energy calculations in this step. We are currently testing our TM prediction algorithm with this thermodynamically based hydrophobicity scale. These calculated hydrophobic penalty values were used to determine which region of angles to choose for each of the six TMs (excluding TM3 which has little direct contact with the lipid bilayer).

The specific residues involved in each interhelical hydrogen bond were identified so that hydrogen bonds involving residues conserved within class A and biogenic amine receptors could be given more importance in choosing angles for combinatorial analysis. The residues focused on were

- ASN71 in helix 1, ASP99 in helix 2, and TRP179 in helix 4 (all highly conserved among class A GPCRs) and
- ASP134 in the center of helix 3, TRP324 in helix 6, and ASN364 in helix 7 (conserved among all mammalian biogenic amine receptors) [27].

Experiments on various GPCRs suggest that the helix 2 aspartic acid forms a hydrogen bonding network with the asparagines in helices 1 and 7 [28,29]. The helix 3 aspartic acid is known to bind the amino functional group in biogenic amines [30]. The helix 4 tryptophan is the most highly conserved residue across the entire GPCR superfamily, and is thought to be integral in structural stabilization [30]. The helix 6 tryptophan is believed to be important in activation [30]. Helix 5 is the least conserved helix in GPCRs, suggesting its role in ligand specificity. A proline is highly conserved among class A GPCRs, but its role is most likely to disrupt the hydrogen bonding within the helix and create flexibility [30]. Thus, it would not necessarily be pointing in to interact with other helices or the ligand.

The list of specific hydrogen bonds formed for each helical rotation is used to help choose angles for combinatorial analysis.

- If a hydrogen bond occurs between two conserved residues, the angles for the two helices are retained.

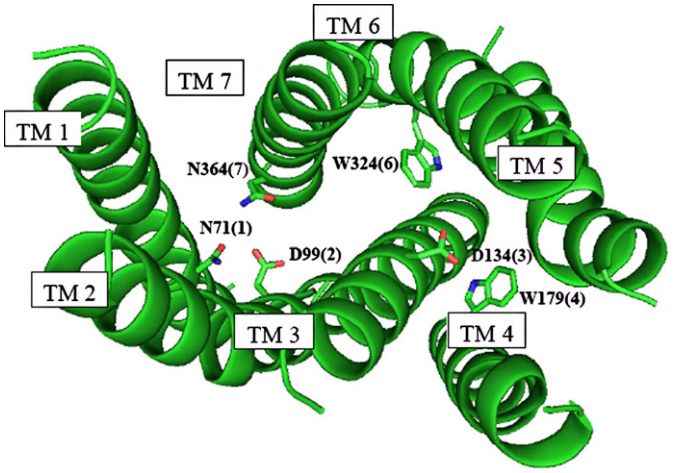

Fig. 1. The final predicted structure of apo-5-HT_{2C}. Indicated explicitly are the six amino acids expected to be involved in important interhelical or ligand-binding interactions.

- If the hydrogen bond involves just one conserved residue, we choose the angle or angles that retain the hydrogen bond and have the best combination of energy, hydrogen bonding and hydrophobic penalty.
- If a helix does not have a conserved residue involved in a hydrogen bond, the angle or angles with the best energy, number of hydrogen bonds and hydrophobic penalty are selected.

The rotational profile for each TM is shown in Supplementary material. Based on this, we selected 0° for TM1; 175° and −125° for TM2; 0°, −20° and −45° for TM3; −50° and −75° for TM4; −35° and −75° for TM5; 90° for TM6; and 170° for TM7. This leads to 24 cases, for each of which we used SCRWL to reassign side-chains and then minimized the energy. These structures were ranked by number of hydrogen bonds and then by energy as shown in Supplementary material. The final rotations for helices 1 through 7 were

0°, −125°, −20°, −50°, −75°, 90°, and 170°.

The lipid and counterions were removed from the final structure and it was fully minimized. The final structure is shown in Fig. 1.

2.5. Prediction of ligand-binding sites

Given the final minimized structure for the apo-protein of 5-HT_{2C}, we then docked various known ligands into the receptor:

- serotonin, the endogenous ligand, an agonist;
- three strongly binding antagonists: ritanserin, metergoline and methiothepin; and
- a series of 10 analogs of psilocybin, both agonists and antagonists.

These ligands are shown in Fig. 2. The ligands were built and minimized (Cerius2) using the Dreiding force field with Mulliken charges from quantum mechanics (B3LYP flavor of DFT using the 6-31G** basis set, calculated with Jaguar). We also calculated the pK_a values for each ligand using the pK_a module of Jaguar to determine if the ligand would be charged, and which atom would become protonated at biological pH 7.4. These pK_a values are listed in Table 4. The docking was done with flexible ligands and a rigid protein.

To search for the best binding site for each ligand, we first alanized the bulky non-polar residues (leucine, isoleucine, valine, phenylalanine, tryptophan and tyrosine). That is, each was mutated to alanine. Then we used the negative of the molecular surface of the alanized protein to define the regions in which to sample different ligand conformation. These void regions were mapped with a set of spheres. Then, we defined 36 boxes, each a cube with 10 Å sides, grown from the center of mass of the spheres and covering the entire receptor. Each ligand was docked (using Dock 4.0) into all 36 boxes and ranked by interaction energy and buried surface. Then, we examined the boxes with a combination of the strongest bonding and buried surface, and selected boxes with a continuous range of spheres for subsequent docking with MSCDock. As an example, the sphere set that the antagonists were docked into is shown in Fig. 3.

We then used MSCDock to dock each ligand into the selected boxes using the dock with diversity method. This method uses Monte Carlo search techniques to find sites that pass bump tests and groups these into families for which all family heads are at least 0.6 Å CRMS different from the others. This is carried out until the number of families is saturated. Then we select the 50 families with the best combination of energy and buried surface and continue generating docking configurations until there is an average of six children in each family. Then we calculate the energy for each child of each of these families, and associate the energy with the family head.

Next for each of these 50 ligand configurations, we de-alanize the bulky non-polar residues back to their original form and reassign all side-chains within 5 Å of the ligand with SCREAM. We minimize (conjugate gradients to 0.2 kcal/molÅ RMS force) the ligand and residues within 5 Å of the ligand with the rest of the protein fixed. Then we minimize the entire complex to 0.2 kcal/molÅ RMS force.

The top 10 structures by total energy of the ligand–protein complex were selected as the best docked structures. From these top 10 structures, we selected the one with the best contacts between the functional groups of the ligand and the residues in the binding site. Then we used SCREAM to reassign the side-chains for the residues interacting most favorably with the functional groups of the ligand to obtain their optimal orientation with respect to the ligand. The ligand and residues within 5 Å were put through one quench-anneal cycle (50–600 K and back over 11.5 ps), selecting the structure with the lowest potential energy structure. This was followed by minimizing the energy of the entire ligand–protein complex.

Serotonin, ritanserin, metergoline and methiothepin were all docked following this procedure. For the 10 SAR ligands, we chose derivative 3 as the template and docked it using the above procedure. Then, we generated a sphere set fitted to a region within 0.8 Å radius around the best docked derivative 3 molecule. Then the entire docking procedure was carried out over this smaller region for the other nine SAR ligands, keeping the bulky residues in place (not mutated to alanines).

3. Molecular dynamics simulation

A simulation was performed on serotonin bound in 5-HT_{2C} in order to determine the stability of the predicted bound structure. NAMD 2.5 [31] was used to perform 5 ns of full solvated lipid bilayer simulation. First, loops were added with a Monte Carlo loop builder. Only the first and last ten residues of the ic3 loop were added. The loops were built so that the disulfide bridge between the two cysteines in ec2 and the top of

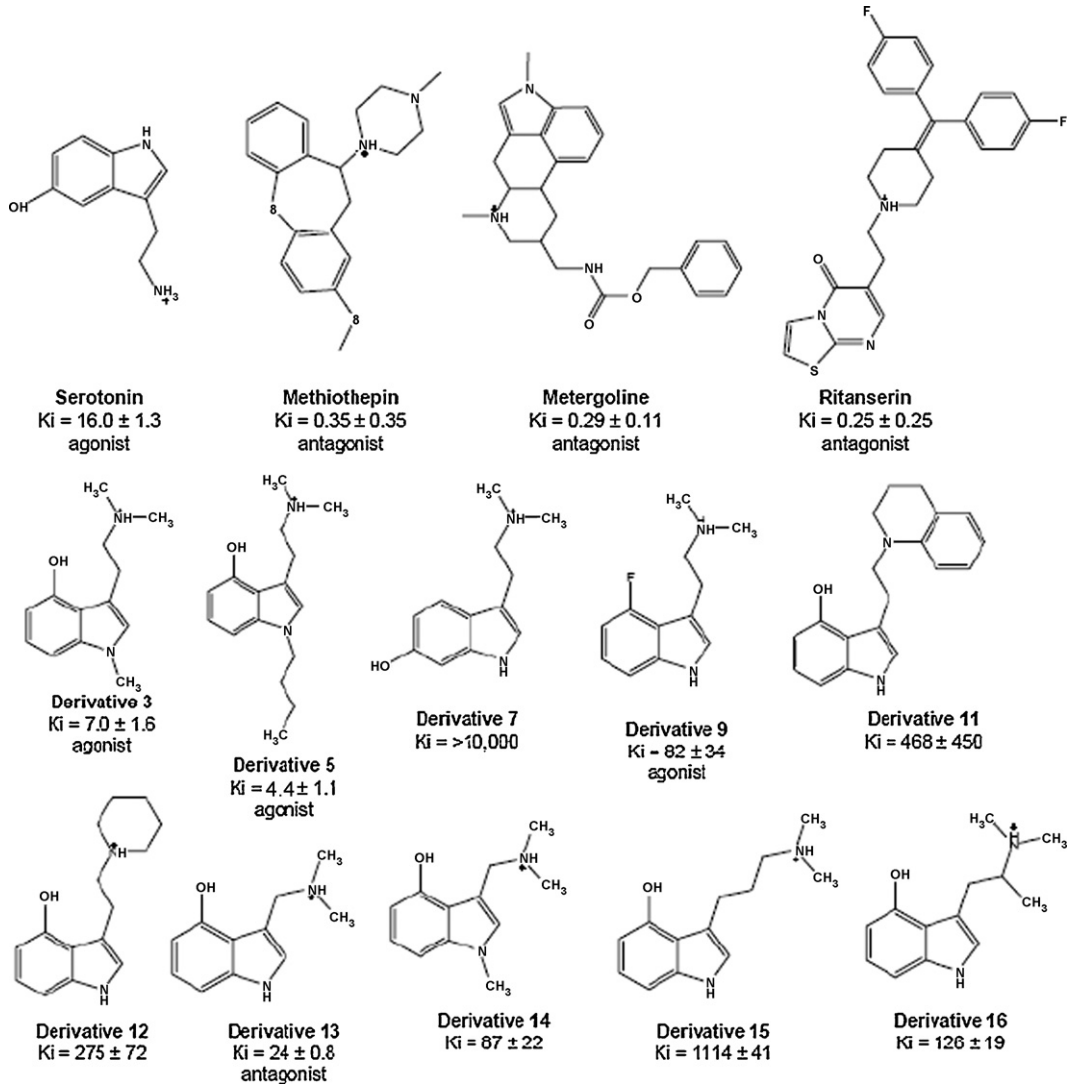

Fig. 2. The structures and experimental binding constants to 5-HT_{2C} for serotonin, three strongly binding antagonists, and a set of psilocybin analogs (derivatives 3–16). The role of the receptor (whether it is an agonist or antagonist) is given if it has been determined experimentally.

TM3 was preserved. Ten residues each of the N-terminus and C-terminus were added. Then, the helices and side-chain were frozen while loops were put through a quench-anneal cycle. Next, palmitoyloleoyl-phosphatidylethanolamine (POPE) lipid molecules were added, along with a layer of water above and below. Chloride ions were added to neutralize the charge of the system. The membrane and water molecules were minimized with the protein fixed, and then equilibrated for 500 ps in an NPT simulation. Then the loops were minimized along with the membrane and water molecules, and equilibrated for 500 ps in an NPT simulation. Finally, the entire system was minimized, and then 5 ns of NPT simulation was run. All NPT simulations were run using Langevin dynamics with a damping coefficient of 1 ps^{-1} and a bath temperature of 310 K. The pressure was kept constant by Nosé-Hoover Langevin piston pressure control, with a target pressure of 1 atm and barostat oscillation and damping times of 200 fs. The stepsize was 1 fs, with periodic boundary conditions applied. Particle mesh Ewald was used for electrostatic calculations, with a nonbond cutoff of 12.0 Å and the nonbonded interactions of all one to three pairs included. The energy and volume of the system equilibrated quickly, as shown in Supplementary material.

3.1. Binding energies calculations

For all the docked structures, the binding energies were calculated as

$$E_{\text{bind}} = E_{\text{comp,vac}} - E_{\text{prot,vac}} - E_{\text{lig,vac}} - E_{\text{lig,solv}}.$$

Since the binding energy is the change in energy upon binding, more negative binding energies indicate stronger binding. The energies of the separate protein and ligand were not re-minimized. That is, they were taken directly from the bound complex (to obtain the snap binding energy). This assumes that there is little change in energy of the separated ligand and protein upon minimization. This also does not take the solvation of the complex or the protein into consideration. However, for small molecules binding in the core of the protein like we are working with, the solvation energy of the bound complex should not differ greatly from that of the unbound protein. The solvation energy of the ligand was calculated using the Poisson–Boltzmann continuum solvent approximation (dielectric constant of 80 and solvent radius of 1.4 Å) using the Delphi program. The vacuum energies were calculated with MPSim, as in all of the structure prediction steps, so the solute dielectric was 2.5.

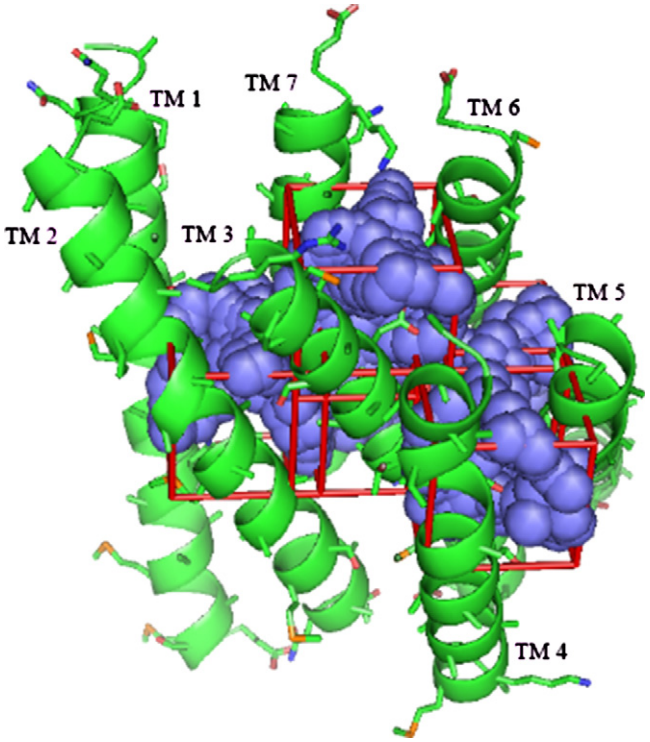

Fig. 3. The boxes containing the spheres into which the antagonists ritanserin, methiothepin and metergoline were docked. All of the bulky, non-polar residues have been alanized.

Next, we neutralized all charged residues of the system and the ligand by transferring the hydrogen of each salt bridge from the acceptor back to the donor and by adding a proton to each exposed Asp or Glu and removing one from each Lys and Arg. We used a modified Dreiding FF that included special hydrogen bonding parameters chosen to reproduce the binding for dimers of analogous residues found from QM. Each full ligand–protein complex was then re-minimized and the binding energies for the neutral forcefield were calculated according to the same equation as for the charged case, but with the addition of a pK_a penalty term. This is the energy change required to neutralize the ligand or residue that prefers to be charged in water solvent. For a positively charged ligand this is equal to 1.4 kcal/mol (pK_a, 7.4).

This modified neutral Dreiding forcefield was also used to calculate the contributions of individual residues to binding. As in all of the other Dreiding calculations, the dielectric constant was 2.5, with van der Waals interactions calculated by a 6–12 Lennard–Jones potential. The nonbond interactions were calculated between the bound ligand and all residues within 5 Å of the ligand.

The neutral residue scheme is an improvement over the charged residue scheme for the binding energy calculations because it decreases the large variations between complexes caused by exaggerated long-range Coulombic interactions between charged groups. These exaggerated interactions are due to the fact that the charges are fixed in molecular mechanics, so charge screening is not present to damp the long-range interactions. Additionally, in the hydrophobic membrane environment, many of the residues may already be neutral. The neutralization procedure is carried out for the binding energy calculations and not the docking procedure because the large Coulombic interactions are important to ensure that binding modes with a salt bridge are selected.

4. Results and discussion

4.1. Serotonin binding

Serotonin is the endogenous agonist to 5-HT_{2C} with a binding constant of K_i = 16.0 nM [32]. The predicted binding site for serotonin to our predicted structure for 5-HT_{2C} is shown in Fig. 4 and the cavity analysis is in Table 2. The most important contacts are

- D134(3) forms a salt bridge with the protonated primary amine site (8.7 kcal/mol), which makes excellent sense. Indeed, experiments suggest that D134(3) creates a salt bridge with the protonated nitrogen of biogenic amines [30].
- The protonated primary amine also forms a hydrogen bond with S138(3) (5.7 kcal/mol).
- The aromatic indole group has very good van der Waals interactions with F223(5) (3.0 kcal/mol) and F328(6) (4.9 kcal/mol). The ring is stacked between the two phenylalanines.
- The polar NH of the indole forms a hydrogen bond with S219(5) (6.5 kcal/mol).
- The OH substituent of the indole forms hydrogen bonds both with S141(3) (3.3 kcal/mol) and W324(6) (2.0 kcal/mol).
- There is good van der Waals interaction between the indole and I332(6) (2.0 kcal/mol).

Overall, the bound structure for serotonin looks reasonable, with each polar functional group of serotonin making favorable

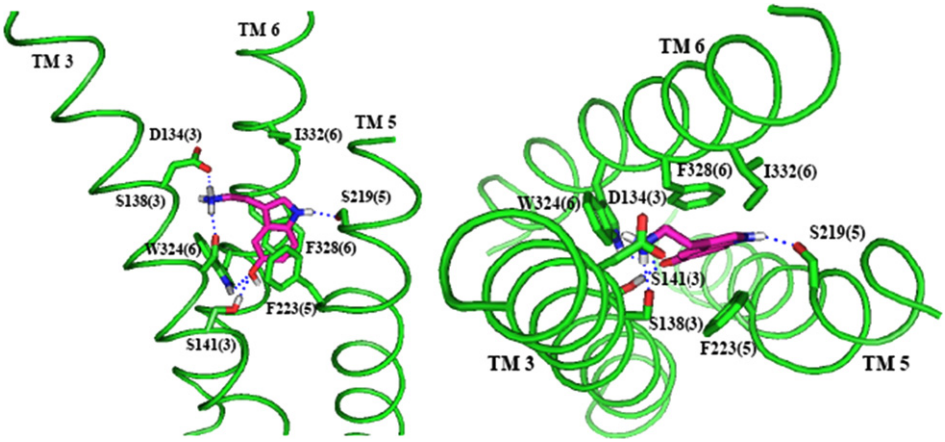

Fig. 4. The predicted structure (side and top views) of serotonin bound to 5-HT_{2C}. TMs 1, 2, 4 and 7 are not shown since they do not interact directly with the ligand. The residues shown are those within 5.0 Å of serotonin that have more than 2 kcal of favorable interaction with the ligand. The dotted lines indicate hydrogen bonds with serotonin. These hydrogen bond distances to the ligand are 1.85 Å to D134, 1.93 Å to S138, 1.94 Å to S141, 1.96 Å to S219 and 2.86 Å to W324.

Table 2
Nonbond interaction energies (kcal/mol) between each ligand and individual residues within 5.0 Å of the ligand

	D134	F328	S219	F223	S138	I332	W324	V215	P190	S141
TM helix no.	3	6	5	5	3	6	6	5	4	3
Ritanserin	−9.6	−0.4	−1.5	−1.6	−0.3	−4.1	−8.5	−3.2	−1.9	0.3
Metergoline	−10.9	−0.5	−1.8	−0.9	−7.4	−1.6	−0.2	−5.9	−4.7	−0.2
Methiothepin	−12.2	−1.5	−6.1	−1.8	−1.3	−0.8	−0.3	−2.3	−3.9	0.0
Deriv 5	−9.8	−6.9	−4.9	−4.3	−2.7	−2.9	−2.4	−0.5	−0.2	0.4
Deriv 3	−9.0	−6.1	−4.8	−6.3	−2.4	−2.3	−1.4	−0.7	−0.2	−1.0
Serotonin	−8.7	−4.9	−6.5	−3.0	−5.7	−2.1	−2.0	−0.3	−0.1	−3.3
Deriv 13	−9.0	−6.6	−5.0	−3.2	−1.2	−1.7	−1.9	−0.3	−0.1	−0.8
Deriv 9	−9.0	−5.9	−1.3	−4.8	−2.1	−3.1	−1.7	−0.3	−0.1	−0.2
Deriv 14	−8.4	−6.4	−4.1	−5.5	−1.3	−1.2	−1.0	−0.5	−0.1	−0.2
Deriv 16	−11.2	−4.8	−4.6	−5.8	−1.2	−2.7	−0.9	−0.6	−0.1	−0.1
Deriv 12	−12.3	−6.1	−5.3	−3.2	−1.5	−3.2	−1.8	−1.6	−0.9	−0.7
Deriv 11	−2.7	−6.1	−5.1	−4.8	−1.6	−1.7	−1.7	−2.8	−1.6	−0.6
Deriv 15	−9.5	−4.4	−0.8	−4.0	−1.8	−2.0	−2.2	−0.1	−0.1	−6.1
Deriv 7	−8.2	−6.3	−1.9	−4.2	−1.6	−2.7	−1.4	−0.7	−0.2	−0.2
Average	−9.3	−4.8	−3.8	−3.8	−2.3	−2.3	−2.0	−1.4	−1.0	−0.9

Here we list only the residues that have more than 2 kcal of favorable energy with at least two ligands. The ligands are ordered by decreasing experimental binding strength (see Table 4).

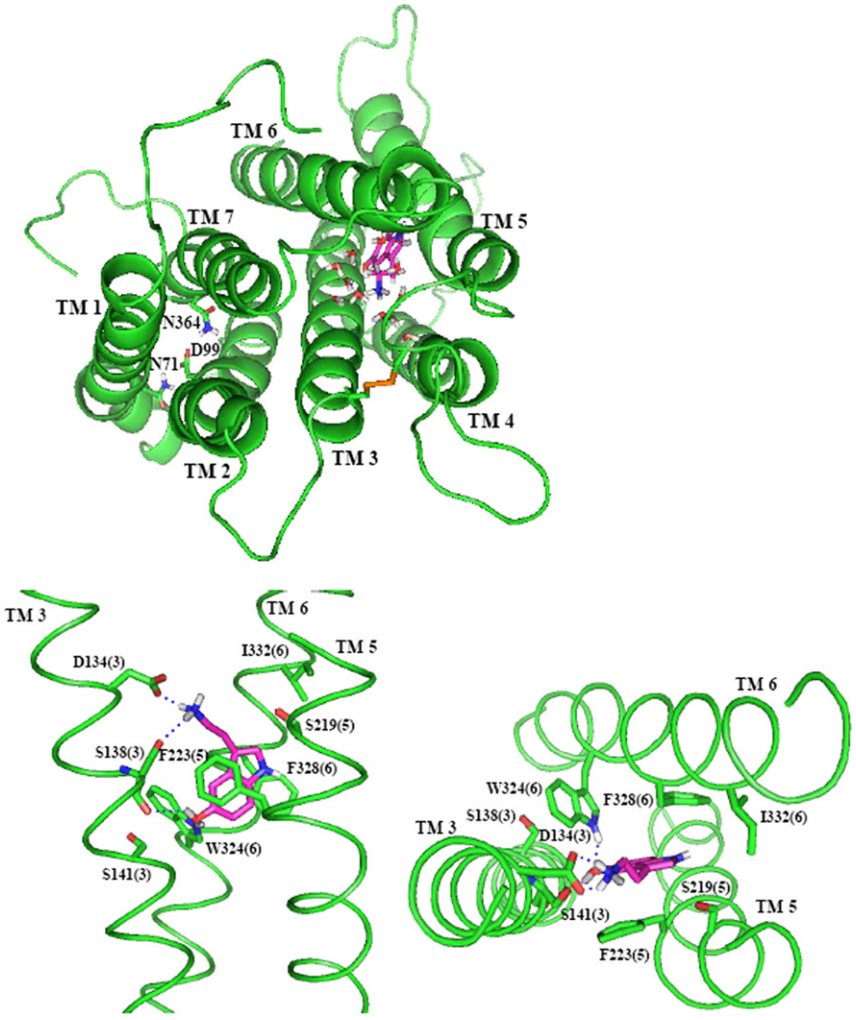

Fig. 5. Serotonin bound in 5-HT_{2C} after 5 ns of dynamics. The top shows the TMs 1-2-7 hydrogen bonding network, as well as the disulfide bond between the two cysteines in TM3 and ec2. The water molecules shown are those within 5.0 Å of serotonin. The bottom shows the binding pocket, with the important residues from the structure before minimization or dynamics. The dotted lines indicate hydrogen bonds with serotonin. The hydrogen bond distances to serotonin are 1.77 Å to D134, 2.00 Å to W324, 2.27 Å to the γ-oxygen of S138 and 2.82 Å to the backbone oxygen of S138.

interactions with a polar or charged residue in the binding pocket and with excellent aromatic interactions.

4.2. Bound serotonin dynamics

In order to determine the stability of this bound structure, we carried out a 5 ns simulation of this complex in an explicit lipid bilayer. This simulation shows the predicted structure and binding site to be stable for 5 ns. Some of the hydrogen bond contacts made with serotonin do change throughout the simulation, but the ligand stays in the same binding site, just moving a little downward towards the intracellular region. The hydrogen bond with S219(5) and the van der Waals interactions with I332(6) are lost as serotonin moves downward. The hydrogen bond with S141(3) is lost as the oxygen of the OH substituent of serotonin forms a very strong hydrogen bond with W324 and the hydrogen of the OH group forms a hydrogen bond with the backbone oxygen of S138(3). Both D134(3) and S138(3) maintain their strong hydrogen bonds with the protonated amine group of serotonin. Additionally, both F223(5) and F328(6) preserve their strong van der Waals interactions with the indole serotonin throughout the simulation. The distances between serotonin and key residues during the simulation are shown in Supplementary material. Waters enter the binding site and accumulate around the salt bridge between D134(3) and serotonin. There were no additional restraints placed on the helices to prevent them from unraveling, so the C-terminus of helix 1 unravelled by two residues, the N-terminus of helix 2 by one residue, the N-terminus of helix 3 by one residue, and the N-terminus of helix 7 by one residue. The TMs 1-2-7 hydrogen bonding network is retained, although the helices do translate with respect to each other during dynamics. The structure after 5 ns is shown in Fig. 5.

4.3. Comparison of predicted serotonin binding site to mutagenesis experiments

Since no experimentally determined structures for any serotonin receptors are available, experimental validation must come from additional mutagenesis studies, in which residues in the active site are mutated to various amino acids and the effect on ligand-binding determined. Many experimental studies have been performed on 5-HT_2 receptors, with the majority of the mutation experiments focused on 5-HT_{2A}. Although there are differences between the receptors, we find 70% sequence identity and 88% sequence similarity between 5-HT_{2A} and 5-HT_{2C} in the predicted TM regions, so it can be useful to compare our predicted structure with experimental findings on 5-HT_{2C}.

- D155(3) in 5-HT_{2A}, which corresponds to D134(3) in 5-HT_{2C} was found to anchor the terminal amine moiety of serotonin [33], as we predict in 5-HT_{2C}.
- An alanine substitution of S159(3) in 5-HT_{2A}, corresponding to S138(3) in 5-HT_{2C}, was found to decrease serotonin binding by 18-fold [34], leading to the proposal that S159(3) forms a hydrogen bond with the protonated amine group of serotonin, just as we predict for 5-HT_{2C}.
- S239(5) in 5-HT_{2A}, which is an alanine in 5-HT_{2C} that is one turn away from S219(5), is proposed to form a hydrogen bond to the polar NH of the indole in serotonin [35]. We predict that in 5-HT_{2C}, the NH of the indole in serotonin forms a hydrogen bond with S219(5), but we find this hydrogen bond to disappear after 5 ns of dynamics.
- F243(5) and F244(5) in 5-HT_{2A} are found to have significant interactions with serotonin, with both predicted to point in towards the binding pocket [36]. F243(5) in 5-HT_{2A} corresponds to F223(5) in 5-HT_{2C}, which we predict to have very good van der Waals interactions with serotonin, but we predict F224(5) not to interact strongly with serotonin in 5-HT_{2C}.
- Mutation of F340(6) to leucine in 5-HT_{2C} significantly decreases serotonin binding, but mutation of F339(6) to leucine did not affect binding [37]. We predict the same effect in 5-HT_{2C} with serotonin making very good van der Waals interactions with F328(6), but not significantly interacting with F327(6).
- Mutation of W336(6) to alanine was found to cause an almost 1000-fold decrease in serotonin binding in 5-HT_{2A} [38]. We predict the corresponding residue in 5-HT_{2C}, W324(6), to have good van der Waals and hydrogen bonding interactions with serotonin.

Our predicted serotonin binding site for 5-HT_{2C} has many similarities to experimentally determined features of the 5-HT_{2A} binding site. A homology model of 5-HT_{2C} based on the crystal structure of bovine rhodopsin [4], produced by the WHAT IF program [39] does not agree with these mutagenesis experiments as well as our predicted structure. TM5 has S219(5) pointed away from the binding pocket, towards TM6. Additionally, D134(3) is pointed towards the 1-2-3-7 pocket instead of the 3-5-6-7 pocket. Thus, serotonin would not bind in the 3-5-6-7 pocket, as expected for biogenic amine receptors [40].

The recently determined experimental structure of the beta(2)-adrenergic receptor [5] has more similarities to our predicted structure for 5-HT_{2C} than does the structure of bovine rhodopsin, but there are still some key differences in the predicted binding site. The TM5 serine in the beta2 structure that corresponds to S219(5) in 5-HT_{2C} is pointing in towards TM3. However, the well-conserved TM3 aspartic acid in beta2 thought to anchor the protonated amine of bound biogenic amines is pointing towards the 1-2-3-7 pocket, as seen in bovine rhodopsin. Thus, in a homology model of 5-HT_{2C} based on the crystal structure of the beta(2)-adrenergic receptor, serotonin cannot make good contacts with both D134(3) and S219(5) like we predict in our structure.

Based on our predicted bound structure and its dynamics, additional experiments that could help validate our predicted binding site are D134A, S138A, F328A, F223A and W324, all of which would lead to significant decreases in serotonin binding affinity. Although the simulation shows the hydrogen bond between serotonin and S219(5) to be absent after 5 ns, it may reappear after a longer simulation, so S219A could also lead to a decrease in serotonin binding affinity.

4.4. Ritanserin antagonist binding

Ritanserin is an antagonist to 5-HT_{2C} with a binding constant of K_i = 0.25 nM [41]. It is used for the treatment of many neurological disorders. The predicted binding site for ritanserin to our predicted structure for to 5-HT_{2C} is shown in Fig. 6 and the cavity analysis is in Table 2. The most important contacts are

- The protonated nitrogen of the piperidine forms a salt bridge with D134(3) (9.6 kcal/mol).
- The oxygen of the pyrimidine makes a hydrogen bond with W324(6) (8.5 kcal/mol).
- The aromatic thiazolo-pyrimidine group has strong van der Waals interactions with F137(3) (4.9 kcal) and N331(6) (2.2 kcal).
- The flourophenyl groups have strong van der Waals interactions with I332(6) (4.1 kcal/mol) and V215(5) (3.5 kcal/mol).

Note that the sulfur of the thaizole does not make strong interactions with polar or charged residues. This suggests that

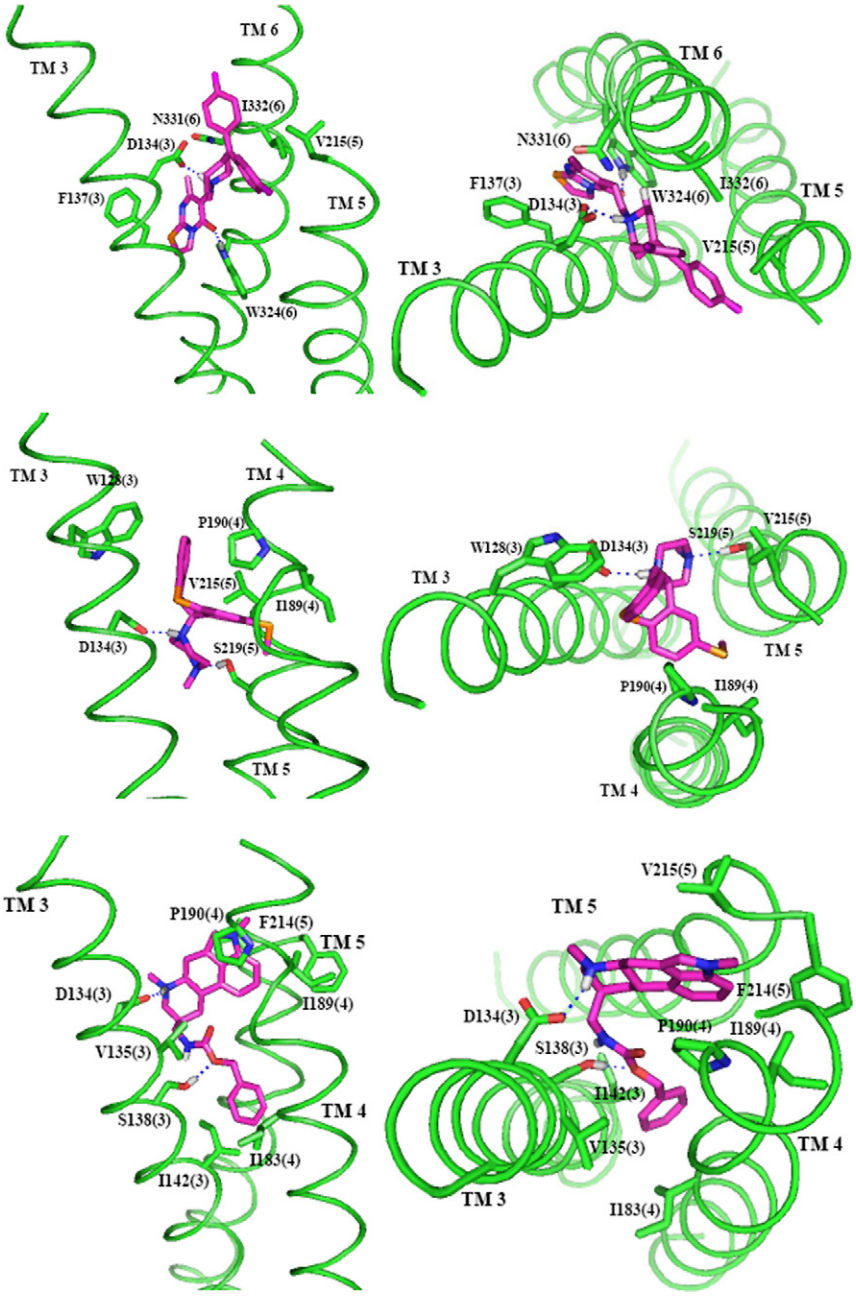

Fig. 6. Side and top views of ritanserin (top), methiothepin (middle) and metergoline (bottom) bound in 5-HT_{2C}. The TMs not shown do not directly interact with the ligand. The residues shown are those within 5.0 Å of the ligand that have more than 2 kcal of favorable interaction with the ligand. The hydrogen bonds formed between the protein and the ligand are indicated by dotted lines. For ritanserin, these distances are 1.97 Å to D134 and 2.04 Å to W324. For methiothepin, the distances are 1.89 Å to D134 and 1.97 Å to S219. The distances for metergoline are 1.90 Å to D134 and 1.95 Å to S138.

improved binding might be obtained by modifying I363(7) or V359(7) to a polar residue able to hydrogen bond with the sulfur. Additionally, the fluorines of the antagonists do not interact strongly polar or charged residues. They may be interacting with the charged head groups of the lipid molecules, water molecules that enter the binding site, or charged or polar residues in the loops.

4.5. Metergoline antagonist binding

Metergoline is an antagonist to 5-HT_{2C} with a binding constant of K_i = 0.29 nM [32]. Metergoline is used as an analgesic in migraine headaches. The predicted binding site for metergoline to our predicted structure for to 5-HT_{2C} is shown in Fig. 6 and the cavity analysis is in Table 2. The most important contacts are

- D134(3) forms a salt bridge with the protonated nitrogen of the ergoline (10.9 kcal/mol).
- Both the N–H group of the amide and the carboxyl oxygen of the ester make hydrogen bonds with S138(3) (7.4 kcal/mol).
- The aromatic ergoline group has strong van der Waals interactions with V215(5) (5.9 kcal/mol), P190(4) (4.7 kcal/mol), F214(5) (2.5 kcal/mol), and I189(4) (2.5 kcal/mol).
- The phenyl group has good van der Waals interactions with I142(3) (2.9 kcal/mol) and I182(4) (2.0 kcal/mol).

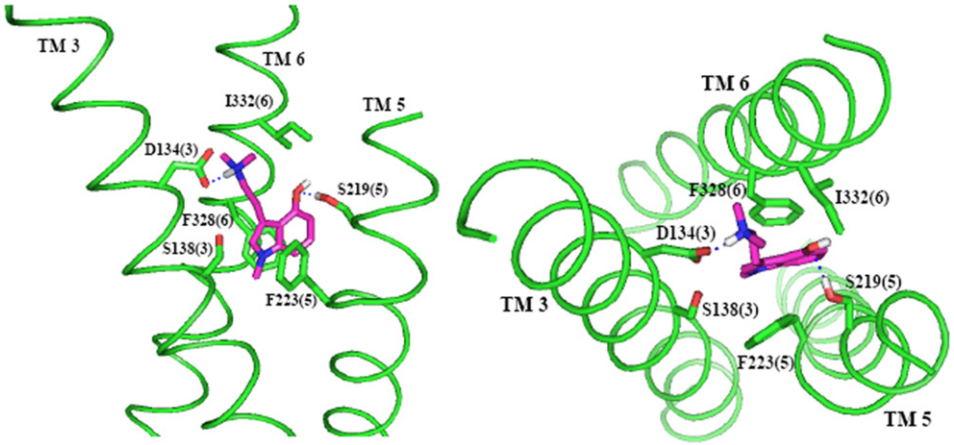

Fig. 7. Side and top views of derivative 3 bound to 5-HT$_{2C}$. The TMs not shown do not directly interact with the ligand. The residues shown are those within 5.0 Å of derivative 3 that have more than 2 kcal of favorable interaction with the ligand. The hydrogen bonds made with the ligand, indicated by the dotted lines, have distances of 1.87 Å to D134 and 1.95 Å to S219.

4.6. Methiothepin antagonist binding

Methiothepin is an antagonist to 5-HT$_{2C}$ with a binding constant of K_i = 0.35 nM [41]. It is used as an antipsychotic. (*S*)-Methiothepin was docked for this study. The predicted binding site for methiothepin to our predicted structure for to 5-HT$_{2C}$ is shown in Fig. 6 and the cavity analysis is in Table 2. The most important contacts are

- D134 interacts with the protonated N at the center of methiothepin (12.2 kcal/mol).
- The piperazine NH forms a hydrogen bond with S219(5) (6.1 kcal/mol).
- The two benzene rings have good van der Waals interactions with P190(4) (−3.9 kcal/mol), W128(3) (2.8 kcal/mol) and V225(5) (2.3 kcal/mol).
- I189(4) has good van der Waals interactions with the thiol ether (2.5 kcal/mol).

Note that sulfur in methiothepin makes strong interactions with neither polar nor charged residues. This suggests that improved binding might be obtained by modifying I131(3), V135(3), G218(5) or I189(4) to polar residues able to form hydrogen bonds with the sulfurs. If S186(4) was modified to an ASN or a THR, it may be long enough to form a hydrogen bond with the thiol ester sulfur.

4.7. SAR for psilocybin analogs

Since there is so little mutation data available for 5-HT$_{2C}$, we will validate our predicted GPCR structure and binding sites by comparing calculated binding energies with experimental binding affinities. Here we consider a series of psilocybin analogs in which small structural changes were found to result in large changes in binding affinity [42]. We carried out full MSCDock docking for derivative 3, to determine the binding mode shown in Fig. 7. The binding modes for the nine other SAR ligands are shown in Supplementary material. The strength of interaction for each ligand with important residues in the binding cavities is given in Table 2.

The binding site of the SAR ligands can explain most of the experimental binding data. All of the ligands form a salt bridge with D134 except derivative 11 which pK_a calculations show to be neutral in solution. Derivatives 3, 5, 11, 12, 13, 14 and 16 form strong hydrogen bonds between the hydroxyl group of the phenol and S219. The position of the hydroxyl group in derivative 7 prevents any hydrogen bonding with S219, which in part leads to its bad binding. The fluorine in derivative 9 that takes the place of the hydroxyl group does not hydrogen bond with S219, but still has favorable interactions with S219, so the binding to 5-HT$_{2C}$ is not as strong as for derivative 3 or 5, but is still fairly strong. In derivatives 13 and 14, the carbon chain is shorter than in serotonin, but this ligand can still form hydrogen bonds with S219. However, they do not bind as strongly as derivatives 3 and 5, which have the same length carbon chain as serotonin. A cavity analysis shows that there are decreased interactions with I332 and S138 in derivatives 13 and 14 compared to derivatives 3 and 5. Derivative 16 also has decreased interaction with S138, caused by the extra methyl group branching from the carbon chain, causing part of the decrease in binding affinity compared to derivative 3. In derivative 15, the length of the carbon chain connecting the protonated amine group and the aromatic rings does not allow for hydrogen bonding with S219, but instead the N–H group of the indole ring forms a hydrogen bond to S141. However, experiments show that derivative 15 does not bind well to 5-HT$_{2C}$, so this hydrogen bond with S141 may not in fact form. S141 could be interacting instead with the backbone of TM3 or forming an interhelical hydrogen bond, maybe with W324, as it does in the dynamics for serotonin bound in 5-HT$_{2C}$. Similarly, the predicted binding site of derivative 12 cannot explain the experimentally observed low binding affinity.

First, consider the trend in total binding energy. We predict derivative 5 to be the best and derivative 7 to be worst, which agrees with experiment. Based on these interactions, proposed mutations that are predicted to decrease significantly the binding affinity of each ligand are listed in Table 3.

- Deriv 3 → 5: This involves replacing the N-Me with N-butyl. Experimentally the binding constant improves from 7.0 to 4.4 nM and we calculate 15% improvement. Our binding site has the butyl in hydrophobic contact with I142(3), I145(3), L227(5) and W324(6) leading to a predicted 4.0 kcal/mol improvement in binding energy over derivative 3. Overall the cavity analysis is quite similar.
- Deriv 3 → 14: This involves removing one CH_2 from the linker connecting the indole with the tertiary amine. Experimentally the binding constant changes from 7.0 to 87 nM and we calculate a 13% weakening in binding. Since the tertiary amine needs to

Table 3
Mutations for each ligand that are predicted to decrease binding affinity

	Proposed mutations to decrease binding affinity
Ritanserin	D134A, W324A, F137A, I332T, V215T
Metergoline	D134A, S138A, V215T, P190S
Methiothepin	D134A, S219A, P190S
Deriv 5	D134A, F328A, S219A, F223A
Deriv 3	D134A, F223A, F328A, S219A
Serotonin	D134A, W324A, S138A, F328A, F223A
Deriv 13	D134A, F328A, S219A, F223A, I332T
Deriv 9	D134A, F328A, F223A, I332T
Deriv 14	D134A, F328A, F223A, S219A
Deriv 16	D134A, F223A, F328A, S219A
Deriv 12	D134A, F328A, S219A, F223A, I332T
Deriv 11	F328A, S219A, F223A
Deriv 15	D134A, S141A, F328A, F223A
Deriv 7	D134A, F328A, F223A

The mutations for each ligand are listed in order of predicted decreasing effect on binding.

keep close to D134(3), the indole is moved slightly away from F223(5), leading to slightly worse binding to both F223(5) and D134(3). Additionally, derivative 3 has better van der Waals interactions with S138(3) and I332(6) than derivative 14. Overall, the cavity analysis is quite similar.

- Deriv 14 → 13: This involves replacing the N-Me of the indole with N–H. Experimentally the binding constant changes from 87 to 24 nM and we calculate a 2% improvement in binding. The difference appears to be from the ligand solvation energy, which is more negative for derivative 14 than derivative 13. Overall, the cavity analysis is quite similar.
- Deriv 13 → 16: This involves adding an extra CHMe to the linker connecting the indole with the tertiary amine. Experimentally the binding constant changes from 24 to 126 nM but we calculate an 8% improvement in binding. Based on the 3 → 14 result we would expect that adding a CH_2 would have improved binding (this compound was not studied experimentally). However, we observe that the OH is farther up in the pocket in derivative 16, creating better van der Waals interactions with I332(6) compared to derivative 13. Additionally, derivative 16 seems to have better van der Waals and Coulombic interactions with D134(3) than derivative 13.
- Deriv 13 → 15: This involves adding two extra CH_2 groups to the linker connecting the indole with the tertiary amine. Experimentally the binding constant changes from 24 to 1114 nM but we calculate a 13% improvement in binding. The extra CH_2 groups on the linker make it so the OH on derivative 15 cannot form a hydrogen bond with S219(5), but instead the NH makes a hydrogen bond with S141(3). However, since derivative 15 does not bind strongly in experiment, this hydrogen bond may not actually exist, and S141(3) may instead interact strongly with W324(6), as seen in the dynamics of serotonin bound to 5-HT_{2C}.

4.8. Discussion of binding energies

The binding energies were calculated for all of the docked ligands and compared to the experimental binding constants in Table 4. Note that binding constants from different experiments cannot be strictly compared because different hot ligands at different concentrations and different temperatures were used. However, we find that very good binders have consistently strong binding constants across different experiments, even though the values are not always the same.

Calculation of binding energies was done for both the charged and neutralized system, and tabulated in Table 4. Using the standard charged model leads to Fig. 8, which plots the predicted binding energies against the logarithm of the experimental binding constants. There is no correlation between the charged binding energies and the K_i values ($R^2 = 0.03$). However, the model in which each residue and ligand is treated as neutral leads to a rather good correlation between the binding energies and the K_i values ($R^2 = 0.70$). Thus, calculating the binding energy with neutral residues and ligands provides a significant improvement over the standard model of charged residues and ligands.

Although the binding energy predictions using neutral residues lead to reasonable correlation with experiment, these calculations are still rudimentary. We consider here minimized structures with continuum solvent approximations. To obtain accurate binding constants we need to carry out molecular dynamics at 300 K and include the entropic contributions to the free energy of binding. Here we must also average the enthalpic parts over the molecular dynamics trajectory while including explicit descriptions of the solvent.

4.9. Comparison to 5-HT_{2B} predictions

The same procedure used to predict the structure of 5-HT_{2C} was used to predict the structure of 5-HT_{2B}. There is a 3.8 Å RMSD between the two predicted structures, whose alignment is seen in Fig. 9. There is close agreement between 5-HT_{2B} and 5-HT_{2C} in the

Table 4
The experimental binding dissociation constants (K_i) and calculated binding energies for ligands bound to 5-HT_{2C}, in order of decreasing experimental binding strength

	Calc pK_a	pK_a pnlt	Vac chrg	Vac neut	Lig solv chrg	Lig solv neut	BE chrg	BE neut	Exper K_i	Exper error
Ritanserin	9.6	3.1	−153.1	−73.4	−59.1	−21.1	−94	−49.2	0.25	±0.25
Metergoline	8.8	2.0	−73.6	−69.7	−51	−18.8	−22.6	−48.9	0.29	±0.11
Methiothepin	9.5	2.9	−49.9	−59.3	−44.5	−11.5	−5.4	−44.9	0.35	±0.35
Deriv 5	9.8	3.4	−86.3	−56.7	−45.1	−8.9	−41.2	−44.4	4.4	±1.1
Deriv 3	9.7	3.2	−86.2	−50.4	−45.9	−8.8	−40.3	−38.4	7	±1.6
Serotonin	9	2.2	−92.2	−52.5	−58	−12	−34.2	−38.3	16.1	±1.3
Deriv 13	10.1	3.8	−78.6	−44.9	−45.5	−6.8	−33.1	−34.3	24	±0.8
Deriv 9	9.6	3.1	−74.9	−42.3	−46.9	−7.6	−28	−31.6	82	±34
Deriv 14	10.1	3.8	−81.8	−45.7	−46	−8.3	−35.8	−33.6	87	±22
Deriv 16	9.7	3.2	−72.2	−47.9	−44.3	−7.5	−27.9	−37.2	126	±19
Deriv 12	10.2	3.9	−83.5	−51.5	−42	−7.1	−41.5	−40.5	275	±72
Deriv 11	4.3	0.0	−46.4	−42.5	−9.6	−9.5	−36.8	−33.0	468	±450
Deriv 15	9.8	3.4	−85.6	−49.9	−49	−7.9	−36.6	−38.6	1114	±41
Deriv 7	9.7	3.2	−78.6	−40.2	−50	−8.8	−28.6	−28.2	10,000	+20,000

More negative binding energies indicate stronger binding. The K_i values and their errors are in units of nM. All energy values are in kcal/mol. The charged binding energy (BE chrg) is defined as the charged vacuum binding energy (vac chrg) minus the solvation energy of the charged ligand (lig solv chrg). The neutral binding energy (BE neut) is the neutral vacuum binding energy (vac neut) minus the solvation energy of the neutralized ligand (lig solv neut) minus the pK_a penalty (pK_a pnlt).

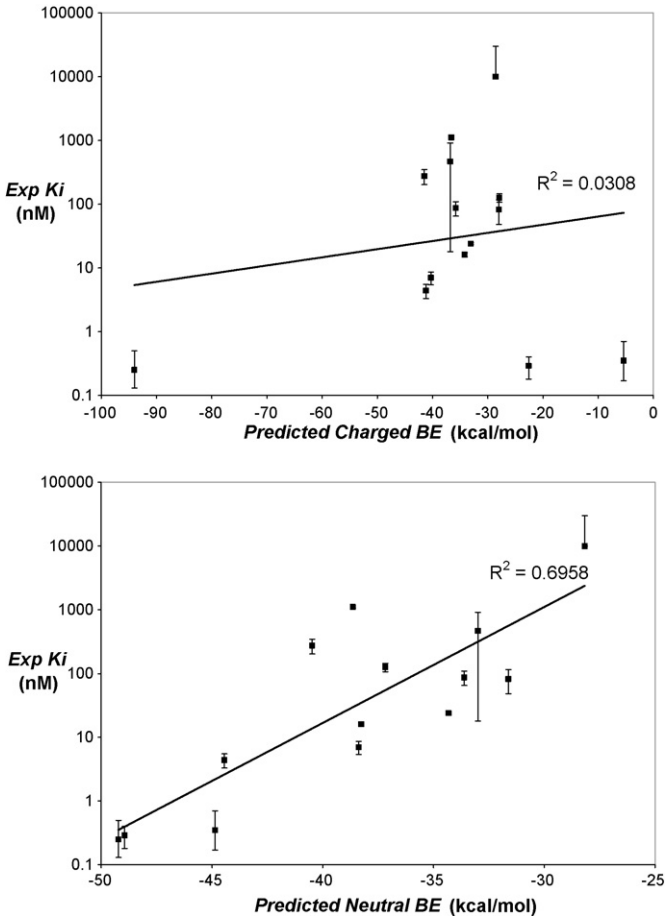

Fig. 8. Predicted charged (top) and neutral (bottom) binding energies vs. experimental binding constants with experimental errors.

rotations of TM1, TM2, TM4, TM6 and TM7. The conserved aspartic acid in TM3 points between TM5 and TM6 in 5-HT_{2C} while it points between TM4 and TM5 in 5-HT_{2B}. In TM5, the conserved serine points into the binding pocket in 5-HT_{2C}, while it points out towards in the membrane in 5-HT_{2B}. Instead, T228 in 5-HT2B TM5, which corresponds to an alanine in 5-HT_{2C}, points towards the binding pocket. TM1 is more bent in 2-HT_{2B} than in 5-HT_{2C} because there is a proline in the middle of the helix in 5-HT_{2B} a turn away from two glycines. TM4 unravels near the end of the helix in both structures because there are two prolines in the helix.

The bound structures for serotonin and ritanserin to 5-HT_{2B} were predicted, and they are shown in Fig. 10. Experimental mutation data for serotonin bound to 5-HT_{2B} can help us assess the accuracy our predicted structure and binding site [43]. Experimentally, serotonin binds to 5-HT_{2B} with a binding constant of K_i = 9.0 nM [44].

- The mutation D135A in TM3 was found to create a greater than 800-fold decrease in serotonin binding affinity to 5-HT_{2B}. This agrees with the prediction that D135(3) creates a salt bridge (16.9 kcal/mol) with the protonated amine of serotonin in 5-HT_{2B}, as it also does in 5-HT_{2C}.
- An alanine substitution of T228(5) was found to cause a 90-fold decrease in serotonin binding affinity to 5-HT_{2B}. Our predicted bound structure sees the OH substituent of the indole in serotonin forming a hydrogen bond with T228(5) (3.0 kcal/mol). The corresponding residue to this TM5 threonine in 5-HT_{2C} is an isoleucine that does not interact with bound serotonin in our predicted structure.

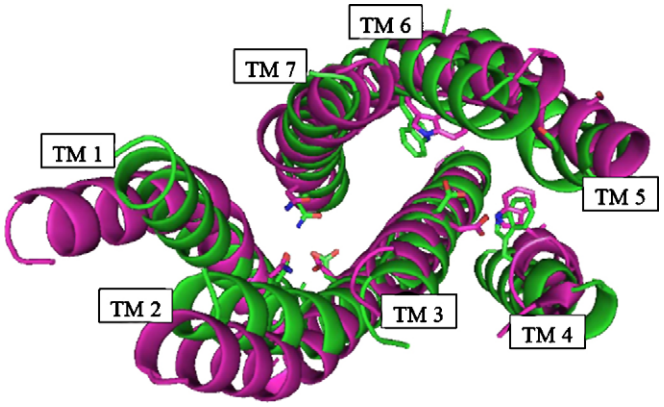

Fig. 9. Alignment of the predicted 5-HT_{2B} and 5-HT_{2C} structures. Indicated explicitly are the conserved residues Asn in TM1, Asp in TM2, Asp in TM3, Trp in TM4, Ser in TM5, TRP in TM6, and Asn in TM7.

- An alanine substitution of S222(5) did not cause any effect on serotonin binding to 5-HT_{2B}. Our predicted bound structure does not have any interaction with this residue. However, we predict the corresponding residue in 5-HT_{2C} to form a hydrogen bond with the polar NH of the indole group in serotonin.
- The mutation F341A in TM6 caused a 15-fold decrease in serotonin binding affinity to 5-HT_{2B} experimentally. Our predicted structure has good van der Waals interactions with F341(6) (3.4 kcal/mol). We predict that the corresponding residue to this in 5-HT_{2C} also has good van der Waals interactions with serotonin.
- An alanine substitution of W337(6) was found to cause a 11-fold decrease in serotonin binding affinity to 5-HT_{2B}. Our predicted structure has moderate interaction with serotonin (1.1 kcal/mol), but this is not high enough to warrant such a large experimental decrease in binding upon mutation. The corresponding tryptophan in 5-HT_{2C} has a stronger predicted interaction with serotonin, forming a hydrogen bond to the OH substituent of the indole in serotonin.
- The mutation S139A in TM3 was found to cause a 30-fold decrease in serotonin binding affinity to 5-HT_{2B}. The predicted structure has moderate interactions (2.1 kcal/mol) between this residue and serotonin, creating a very weak hydrogen bond with the protonated amine of serotonin. The corresponding residue in 5-HT_{2C} has a stronger interaction with the protonated amine of serotonin.
- The substitution of serine for A187(4) was not found to have any effect on serotonin binding affinity to 5-HT_{2B}. We predict little interaction between this residue and serotonin, but we do predict strong hydrogen bonding between the backbone of I188(4) and the protonated amine of serotonin. We predict no such interaction in 5-HT_{2C}. However, this may be an artefact of the excessive unravelling of helix 4 dues to prolines.
- The mutation N344A in TM6 was found to cause a sevenfold decrease in serotonin binding affinity to 5-HT_{2B}. We do not see any interaction between this residue in our predicted structure and serotonin. However, N344(6) is forming a hydrogen bond with W367(7), so it may be involved in structural stabilization instead of ligand binding. These residues are also found in 5-HT_{2C}, but they are not predicted to hydrogen bond.
- The mutation D100N in TM2 was found to cause a 12-fold decrease in serotonin binding to 5-HT_{2B}. D100N(2) does not have any predicted interactions with bound serotonin. However, the double mutation D100N in TM2 along with N367D in TM7 has no effect in serotonin binding. Many studies suggest these helices do not directly bind to serotonin, but instead interact through a

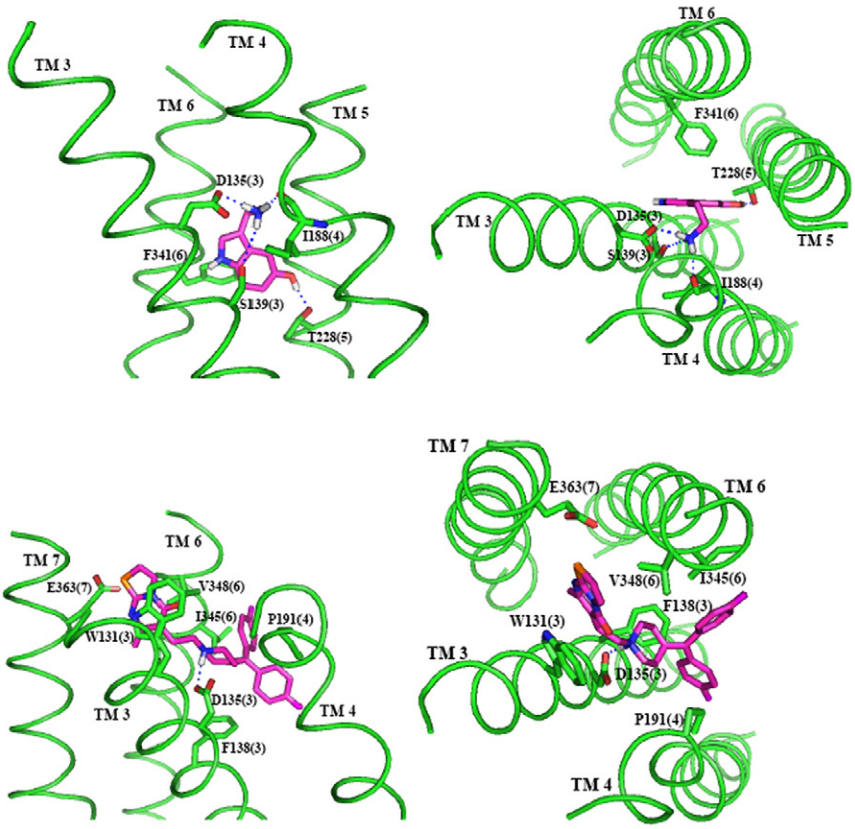

Fig. 10. The predicted structure (side and top views) of serotonin (top) and ritanserin (bottom) bound to 5-HT_{2B}. The TMs shown do not interact directly with the ligand. The residues shown are those within 5.0 Å of serotonin that have more than 2 kcal of favorable interaction with the ligand. The dotted lines indicate hydrogen bonds with the ligand. For serotonin, these distances are 1.86 Å to D135(3), 1.90 Å to I188(4), 3.06 Å to S139(3), and 1.93 Å to T228(5). For ritanserin, the distance to D135(3) is 1.95 Å.

hydrogen bonding network to indirectly affect binding through a conformational change in the binding pocket. This hypothesis is supported by the fact that D100(2) and N376(7) are hydrogen bonding in the predicted structure, and experiments show that if the identities of the two amino acids are switched, effectively retaining the hydrogen bond, the original binding constants to serotonin are maintained. These two amino acids are also hydrogen bonded in 5-HT_{2C}, with no interaction with serotonin.

Comparison of the predicted 5-HT_{2B} serotonin bound structure to mutagenesis experiments shows some good agreement with experiment, but there are also some discrepancies. The fact that serotonin makes a hydrogen bond with the backbone of TM4 probably means that the helix 4 is packed too closely to helix 3, or that helix 4 has unravelled too much. Also, mutagenesis experiments suggest stronger interactions between serotonin and the residues S139(3) and W337(6). There could be hydrogen bonding to S139(3) and better van der Waals interactions with serotonin if helix 3 were rotated more closely to the same angle as it is in 5-HT_{2C}. Despite these inconsistencies, there are strong similarities to the predicted 5-HT_{2C} structure, with the differences in predicted serotonin binding between the two receptors primarily due to the different rotation of TM5.

Our predicted serotonin binding site for 5-HT_{2B} agrees more closely with mutagenesis experiments than do homology models of 5-HT_{2B}. A study comparing homology models of 5-HT based on bacteriorhodopsin and bovine rhodopsin concluded that the bacteriorhodopsin-based model correlated better with experimental mutagenesis data [43]. According to this bacteriorhodopsin-based homology model of 5-HT_{2B}, D135(3), S139(3), F341(6) and N344(6) make direct contacts with serotonin. Additionally, W131(3), F138(3), F341(6) and F365(7) form an aromatic box surrounding serotonin in the homology model. This model does not show any significant interaction between serotonin and TM5, while our model shows hydrogen bonding between serotonin and T228(5). Experiments suggest that T228(5) is very important in binding serotonin, as evidenced by the fact that a mutation to alanine causes a 90-fold decrease in serotonin binding. The homology model has serotonin forming a hydrogen bond with N344(6) instead of with T228(5), although experiments only show

Table 5
The experimental binding dissociation constants (K_i) and calculated binding energies for ligands bound to 5-HT_{2B}, in order of decreasing experimental binding strength

	Calc pK_a	pK_a pnlt	Vac chrg	Vac neut	Lig solv chrg	Lig solv neut	BE chrg	BE neut	Exper K_i	Exper error
Ritanserin	9.6	3.1	−127.4	−60.4	−56.7	−20.9	−70.7	−36.4	1.6	±0.7
Serotonin	9	2.2	−108.7	−46.7	−57.5	−11	−51.2	−33.5	9	±1.9

More negative binding energies indicate stronger binding. The K_i values and their errors are in units of nM. All energy values are in kcal/mol. The charged binding energy (BE chrg) is defined as the charged vacuum binding energy (vac chrg) minus the solvation energy of the charged ligand (lig solv chrg). The neutral binding energy (BE neut) is the neutral vacuum binding energy (vac neut) minus the solvation energy of the neutralized ligand (lig solv neut) minus the pK_a penalty (pK_a pnlt).

a sevenfold decrease of binding from the N344A mutation. Additionally, the homology model shows no interaction with W337(6), while our model has moderate interactions the residue, which agrees with experiment, because the W337A mutation causes a 12-fold decrease in serotonin binding. Thus, overall, our predicted serotonin binding site of 5-HT_{2B} correlates better with the available experimental data than does a bacteriorhodopsin-based homology model.

The binding site for one antagonist, ritanserin, was predicted for 5-HT_{2B}. Experimentally, ritanserin binds to 5-HT_{2B} with a binding constant of K_i = 1.6 nM [44]. The most important contacts are

- The protonated nitrogen of the piperidine forms a salt bridge with D135(3) (16.4 kcal/mol).
- The aromatic thiazolo-pyrimidine group has strong van der Waals interactions with W131(3) (7.8 kcal/mol), V348(6) (5.0 kcal/mol), and E363(7) (2.1 kcal/mol).
- The flourophenyl groups have strong van der Waals interactions with I345(6) (3.2 kcal/mol), P191(4) (2.6 kcal/mol), and F138(3) (2.0 kcal/mol).

This predicted binding site for ritanserin in 5-HT_{2B} has little in common with the predicted binding site for ritanserin in 5-HT_{2C}, except that they both interact with TM3 and TM6, and both have salt bridges between ritanserin and the aspartic acid on TM3.

The binding constants were calculated for serotonin and ritanserin bound to 5-HT_{2B}, and the results are shown in Table 5. The calculated binding constants correctly predict that ritanserin binds more strongly than serotonin to 5-HT_{2B}. When the calculated binding constants for 5-HT_{2B} are compared with those for 5-HT_{2C}, the binding constants for 5-HT_{2C} are stronger than those for 5-HT_{2B}. However, the binding constants for the two receptors are much closer together once the complexes are neutralized.

5. Conclusion

We find good agreement between the calculated binding sites of the predicted ligand–protein bound complexes of 5-HT_{2C} and experimental binding constants. We also find many similarities between the predicted serotonin binding site for 5-HT_{2C} and mutagenesis experiments for 5-HT_{2A}. Additionally, comparison of the predicted 5-HT_{2C} structure with a preliminary prediction of the 5-HT_{2B} structure along with mutation experiments on serotonin bound in 5-HT_{2B} reveals a great deal of similarity between the two structures. This suggests that the 3D protein structure predicted by the MembStruk method is sufficiently accurate for drug design. Dynamics of serotonin bound in 5-HT_{2C} in an explicit lipid bilayer show the predicted binding site to be stable during 5 ns of simulation. The predicted binding site for serotonin leads to the suggested mutations S138A, S141A, S219A, F223A, F328A and W324A and I332A which are predicted to all cause a decrease in binding energies. Mutation experiments for other ligands, including strongly binding antagonists and a series of psilocybin analogs, are also proposed. Thus, a wealth of data is now available to further validate the proposed structure and binding sites of 5-HT_{2C}. The good agreement between experiment and the predicted bound structures indicates that the procedures are useful for studying other systems with less experimental data.

Acknowledgement

We thank the Department of Energy for the award of a Computational Science Graduate Fellowship.

Appendix A. Supplementary data

Supplementary data associated with this article can be found, in the online version, at doi:10.1016/j.jmgm.2008.02.006.

References

[1] B.L. Roth, D.L. Willins, K. Kristiansen, W.K. Kroeze, 5-Hydroxytryptamine(2)-family receptors (5-hydroxytryptamine(2A), 5-hydroxytryptamine(2B), 5-hydroxytryptamine(2C)): where structure meets function, Pharmacol. Ther. 79 (1998) 231–257.
[2] J.E. Leysen, 5-HT_2 receptors, Current drug targets—CNS and neurological disorders 3 (2004) 11–26.
[3] B.L. Roth, E. Lopez, S. Patel, W.K. Kroeze, The multiplicity of serotonin receptors: uselessly diverse molecules or an embarrassment of riches? Neuroscientist 6 (2000) 252–262.
[4] K. Palczewski, T. Kumasaka, T. Hori, C.A. Behnke, H. Motoshima, B.A. Fox, I. Le Trong, D.C. Teller, T. Okada, R.E. Stenkamp, M. Yamamoto, M. Miyano, Crystal structure of rhodopsin: a G protein-coupled receptor, Science 289 (2000) 739–745.
[5] V. Cherezov, D.M. Rosenbaum, M.A. Hanson, S.G.F. Rasmussen, F.S. Thian, T.S. Kobilka, H.J. Choi, P. Kuhn, W.I. Weis, B.K. Kobilka, R.C. Stevens, High-resolution crystal structure of an engineered human beta(2)-adrenergic G protein-coupled receptor, Science 318 (2007) 1258–1265.
[6] W.B. Floriano, S. Hall, N. Vaidehi, U. Kim, D. Drayna, W.A. Goddard, Modeling the human PTC bitter-taste receptor interactions with bitter tastants, J. Mol. Model. 12 (2006) 931–941.
[7] N. Vaidehi, S. Schlyer, R.J. Trabanino, W.B. Floriano, R. Abrol, S. Sharma, M. Kochanny, S. Koovakat, L. Dunning, M. Liang, J.M. Fox, F.L. de Mendonca, J.E. Pease, W.A. Goddard, R. Horuk, Predictions of CCR1 chemokine receptor structure and BX 471 antagonist binding followed by experimental validation, J. Biol. Chem. 281 (2006) 27613–27620.
[8] P. Hummel, N. Vaidehi, W.B. Floriano, S.E. Hall, W.A. Goddard, Test of the binding threshold hypothesis for olfactory receptors: explanation of the differential binding of ketones to the mouse and human orthologs of olfactory receptor 912-93, Protein Sci. 14 (2005) 703–710.
[9] S.E. Hall, W.B. Floriano, N. Vaidehi, W.A. Goddard, Predicted 3-D structures for mouse 17 and rat 17 olfactory receptors and comparison of predicted odor recognition profiles with experiment, Chem. Senses 29 (2004) 595–616.
[10] W.B. Floriano, N. Vaidehi, W.A. Goddard, Making sense of olfaction through predictions of the 3-D structure and function of olfactory receptors, Chem. Senses 29 (2004) 269–290.
[11] R.J. Trabanino, S.E. Hall, N. Vaidehi, W.B. Floriano, V.W.T. Kam, W.A. Goddard, First principles predictions of the structure and function of G-protein-coupled receptors: validation for bovine rhodopsin, Biophys. J. 86 (2004) 1904–1921.
[12] M.Y.S. Kalani, N. Vaidehi, S.E. Hall, R.J. Trabanino, P.L. Freddolino, M.A. Kalani, W.B. Floriano, V.W.T. Kam, W.A. Goddard, The predicted 3D structure of the human D2 dopamine receptor and the binding site and binding affinities for agonists and antagonists, Proc. Natl. Acad. Sci. U.S.A. 101 (2004) 3815–3820.
[13] P.L. Freddolino, M.Y.S. Kalani, N. Vaidehi, W.B. Floriano, S.E. Hall, R.J. Trabanino, V.W.T. Kam, W.A. Goddard, Predicted 3D structure for the human beta 2 adrenergic receptor and its binding site for agonists and antagonists, Proc. Natl. Acad. Sci. U.S.A. 101 (2004) 2736–2741.
[14] N. Vaidehi, W.B. Floriano, R. Trabanino, S.E. Hall, P. Freddolino, E.J. Choi, G. Zamanakos, W.A. Goddard, Prediction of structure and function of G protein-coupled receptors, Proc. Natl. Acad. Sci. U.S.A. 99 (2002) 12622–12627.
[15] A.E. Cho, J.A. Wendel, N. Vaidehi, P.M. Kekenes-Huskey, W.B. Floriano, P.K. Maiti, W.A. Goddard, The MPSim-Dock hierarchical docking algorithm: application to the eight trypsin inhibitor cocrystals, J. Comput. Chem. 26 (2005) 48–71.
[16] K.T. Lim, S. Brunett, M. Iotov, R.B. McClurg, N. Vaidehi, S. Dasgupta, S. Taylor, W.A. Goddard, Molecular dynamics for very large systems on massively parallel computers: the MPSim program, J. Comput. Chem. 18 (1997) 501–521.
[17] S.L. Mayo, B.D. Olafson, W.A. Goddard, Dreiding—a generic force-field for molecular simulations, J. Phys. Chem. 94 (1990) 8897–8909.
[18] D. Donnelly, J.P. Overington, T.L. Blundell, The prediction and orientation of alpha-helices from sequence alignments—the combined use of environment-dependent substitution tables, Fourier-transform methods and helix capping rules, Protein Eng. 7 (1994) 645–653.
[19] S.F. Altschul, T.L. Madden, A.A. Schaffer, J.H. Zhang, Z. Zhang, W. Miller, D.J. Lipman, Gapped BLAST and PSI-BLAST: a new generation of protein database search programs, Nucleic Acids Res. 25 (1997) 3389–3402.
[20] R. Chenna, H. Sugawara, T. Koike, R. Lopez, T.J. Gibson, D.G. Higgins, J.D. Thompson, Multiple sequence alignment with the Clustal series of programs, Nucleic Acids Res. 31 (2003) 3497–3500.
[21] D. Eisenberg, R.M. Weiss, T.C. Terwilliger, The helical hydrophobic moment—a measure of the amphiphilicity of a helix, Nature 299 (1982) 371–374.
[22] G.F.X. Schertler, Structure of rhodopsin, Eye. 12 (1998) 504–510.
[23] M.J. Bower, F.E. Cohen, R.L. Dunbrack, Prediction of protein side-chain rotamers from a backbone-dependent rotamer library: a new homology modeling tool, J. Mol. Biol. 267 (1997) 1268–1282.
[24] A.M. Mathiowetz, A. Jain, N. Karasawa, W.A. Goddard, Protein simulations using techniques suitable for very large systems—the cell multipole method for non-

bond interactions and the Newton–Euler inverse mass operator method for internal coordinate dynamics, Proteins-Struct. Funct. Genet. 20 (1994) 227–247.
[25] S. Jayasinghe, K. Hristova, S.H. White, Energetics, stability, and prediction of transmembrane helices, J. Mol. Biol. 312 (2001) 927–934.
[26] W.C. Wimley, S.H. White, Experimentally determined hydrophobicity scale for proteins at membrane interfaces, Nat. Struct. Biol. 3 (1996) 842–848.
[27] W.K. Kroeze, K. Kristiansen, B.L. Roth, Molecular biology of serotonin receptors—structure and function at the molecular level, Curr. Top. Med. Chem. 2 (2002) 507–528.
[28] J.A. Ballesteros, L. Shi, J.A. Javitch, Structural mimicry in G protein-coupled receptors: implications of the high-resolution structure of rhodopsin for structure–function analysis of rhodopsin-like receptors, Mol. Pharmacol. 60 (2001) 1–19.
[29] M. Eilers, V. Hornak, S.O. Smith, J.B. Konopka, Comparison of Class A and D G protein-coupled receptors: common features in structure and activation, Biochemistry 44 (2005) 8959–8975.
[30] R.P. Bywater, Location and nature of the residues important for ligand recognition in G-protein coupled receptors, J. Mol. Recogn. 18 (2005) 60–72.
[31] J.C. Phillips, R. Braun, W. Wang, J. Gumbart, E. Tajkhorshid, E. Villa, C. Chipot, R.D. Skeel, L. Kale, K. Schulten, Scalable molecular dynamics with NAMD, J. Comput. Chem. 26 (2005) 1781–1802.
[32] J.L. Xie, S. Dernovici, P. Ribeiro, Mutagenesis analysis of the serotonin 5-HT2C receptor and a *Caenorhabditis elegans* 5-HT2 homologue: conserved residues of helix 4 and helix 7 contribute to agonist-dependent activation of 5-HT2 receptors, J. Neurochem. 92 (2005) 375–387.
[33] K. Kristiansen, W.K. Kroeze, D.L. Willins, E.I. Gelber, J.E. Savage, R.A. Glennon, B.L. Roth, A highly conserved aspartic acid (Asp-155) anchors the terminal amine moiety of tryptamines and is involved in membrane targeting of the 5-HT2A serotonin receptor but does not participate in activation via a ''salt-bridge disruption'' mechanism, J. Pharmacol. Exp. Ther. 293 (2000) 735–746.
[34] N. Almaula, B.J. Ebersole, D.Q. Zhang, H. Weinstein, S.C. Sealfon, Mapping the binding site pocket of the serotonin 5-hydroxytryptamine(2A) receptor—Ser(3.36(159)) provides a second interaction site for the protonated amine of serotonin but not of lysergic acid diethylamide or bufotenin, J. Biol. Chem. 271 (1996) 14672–14675.
[35] B.J. Ebersole, I. Visiers, H. Weinstein, S.C. Sealfon, Molecular basis of partial agonism: orientation of indoleamine ligands in the binding pocket of the human serotonin 5-HT2A receptor determines relative efficacy, Mol. Pharmacol. 63 (2003) 36–43.
[36] D.A. Shapiro, K. Kristiansen, W.K. Kroeze, B.L. Roth, Differential modes of agonist binding to 5-hydroxytryptamine(2A) serotonin receptors revealed by mutation and molecular modeling of conserved residues in transmembrane region 5, Mol. Pharmacol. 58 (2000) 877–886.
[37] M.S. Choudhary, S. Craigo, B.L. Roth, A single point mutation (Phe-340-]Leu-340) of a conserved phenylalanine abolishes 4-[I-125]iodo-(2,5-dimethoxy)phenylisopropylamine and [H-3] mesulergine but not [H-3] ketanserin binding to 5-hydroxytryptamine(2) receptors, Mol. Pharmacol. 43 (1993) 755–761.
[38] B.L. Roth, M. Shoham, M.S. Choudhary, N. Khan, Identification of conserved aromatic residues essential for agonist binding and second messenger production at 5-hydroxytryptamine(2A) receptors, Mol. Pharmacol. 52 (1997) 259–266.
[39] G. Vriend, What if—a molecular modeling and drug design program, J. Mol. Graph. 8 (1990) 52–56.
[40] A.M. vanRhee, K.A. Jacobson, Molecular architecture of G protein-coupled receptors, Drug Dev. Res. 37 (1996) 1–38.
[41] D.W. Bonhaus, K.K. Weinhardt, M. Taylor, A. Desouza, P.M. McNeeley, K. Szczepanski, D.J. Fontana, J. Trinh, C.L. Rocha, M.W. Dawson, L.A. Flippin, R.M. Eglen, RS-102221: a novel high affinity and selective, 5-HT2C receptor antagonist, Neuropharmacology 36 (1997) 621–629.
[42] H. Sard, G. Kumaran, C. Morency, B.L. Roth, B.A. Toth, P. He, L. Shuster, SAR of psilocybin analogs: discovery of a selective 5-HT2C agonist, Bioorg. Med. Chem. Lett. 15 (2005) 4555–4559.
[43] P. Manivet, B. Schneider, J.C. Smith, D.S. Choi, L. Maroteaux, O. Kellermann, J.M. Launay, The serotonin binding site of human and murine 5-HT2B-receptors—molecular modeling and site-directed mutagenesis, J. Biol. Chem. 277 (2002) 17170–17178.
[44] D.B. Wainscott, D.A. Sasso, J.D. Kursar, M. Baez, V. Lucaites, D.L. Nelson, [3H]Rauwolscine: an antagonist radioligand for the cloned human 5-hydroxytryptamine2B (5-HT2B) receptor, Naunyn-Schmiedeberg's Arch. Pharmacol. 357 (1998) 17–24.